

Cite this: DOI: 10.1039/c0cp01491e

www.rsc.org/pccp

PAPER

Mapping the frontier electronic structures of triphenylamine based organic dyes at TiO₂ interfaces

Maria Hahlin,^{*a} Michael Odelius,^b Martin Magnuson,^c Erik M. J. Johansson,^d Stefan Plogmaker,^a Daniel P. Hagberg,^e Licheng Sun,^e Hans Siegbahn^a and Håkan Rensmo^{*a}

Received 13th August 2010, Accepted 8th November 2010

DOI: 10.1039/c0cp01491e

The frontier electronic structures of a series of organic dye molecules containing a triphenylamine moiety, a thiophene moiety and a cyanoacrylic acid moiety have been investigated by photoelectron spectroscopy (PES), X-ray absorption spectroscopy (XAS), X-ray emission spectroscopy (XES) and resonant photoelectron spectroscopy (RPES). The experimental results were compared to electronic structure calculations on the molecules, which are used to confirm and enrich the assignment of the spectra. The approach allows us to experimentally measure and interpret the basic valence energy level structure in the dye, including the highest occupied energy level and how it depends on the interaction between the different units. Based on N 1s X-ray absorption and emission spectra we also obtain insight into the structure of the excited states, the molecular orbital composition and dynamics. Together the results provide an experimentally determined energy level map useful in the design of these types of materials. Included are also results indicating femtosecond charge redistribution at the dye/TiO₂ interface.

1. Introduction

Generally molecules containing a triphenylamine moiety are common in molecular electronic applications and a specific focus in the present investigation are dye molecules adsorbed at nanostructured TiO₂ for the potential use in conversion from light to electric energy. Dye-sensitized solar cells (DSC) have received widespread interest as a promising alternative to conventional solar cells. The most efficient DSCs, with efficiencies reaching over 10%, use metal complexes, such as ruthenium polypyridines (N3, N719 and black dye), as light harvesting material, and a liquid based electrolyte containing the redox couple I⁻/I₃⁻ as redox mediator.^{1–3} In recent years there has been an increasing interest in organic dyes as light harvesting materials.^{4–19} The relatively easy synthetic routes of organic dyes makes them easy to modify with respect to the

position of the energy levels important for the DSC energy conversion.

In focus of this investigation is a series of organic dyes, which has proven to yield respectable DSC efficiencies. The dyes in this investigation are constructed using three units, the triphenylamine moiety (referred to as the D5 unit or D9 unit depending on the presence of methoxy units), a thiophene linker moiety (referred to as the L2 unit), and the cyanoacrylic acid anchor moiety (referred to as the A1 unit). The molecular surface structure of this family of dyes when adsorbed on TiO₂ substrates has been investigated previously.²⁰ A goal of this investigation is to understand the contribution of each unit to the total electronic composition and, in doing so, to contribute to further understanding in the field of the molecular dye design.

In the present study we use photoelectron spectroscopy (PES), resonant photoelectron spectroscopy (RPES), X-ray emission spectroscopy (XES), and X-ray absorption spectroscopy (XAS) in combination with theoretical calculations to compare in detail the frontier electronic structure of the organic dyes D9L2A1, D5L2A1, D5A1, and L2A1, see Fig. 1. PES, XES, and RPES are used to probe the occupied electronic structure and XAS is used to probe the unoccupied orbitals. RPES also allows us to relate information in the occupied and unoccupied levels. The experiments are compared to DFT calculations on single molecules. All these techniques taken together give a detailed characterization of the energy level structure within a molecular layer adsorbed on a TiO₂ surface.^{21–26}

^a Molecular and Condensed Matter Physics, Department of Physics and Astronomy, Uppsala University, Box 516, SE-751 20 Uppsala, Sweden. E-mail: Hakan.Rensmo@fysik.uu.se; Fax: +46 18 471 5999; Tel: +46 18 471 3547

^b Department of Physics, Stockholm University, AlbaNova University Center, 106 91 Stockholm, Sweden

^c Department of Physics, Chemistry and Biology (IFM), Thin Film Physics Division, Linköping University, SE-581 83 Linköping, Sweden

^d Department of Physical and Analytical Chemistry, Uppsala University, Box 259, 751 05 Uppsala, Sweden

^e Center of Molecular Devices, Royal Institute of Technology, Chemical Science and Engineering, Organic Chemistry, 100 44 Stockholm, Sweden

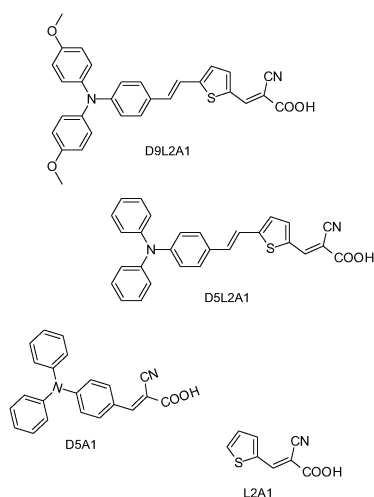


Fig. 1 Molecular structures of D9L2A1, D5L2A1, D5A1, and L2A1.

2. Experimental

2.1 Sample preparation

The synthesis procedure of the 3-(5-bis(4,4'-(methoxyphenyl)amino)styryl)thiophen-2-yl)-2-cyanoacrylic acid (D9L2A1), 3-(5-(4-(diphenylamino)styryl)thiophen-2-yl)-2-cyanoacrylic acid (D5L2A1), 4-(diphenylamino)phenylcyanoacrylic acid (D5A1), and (thiophene-2-yl)-2-cyanoacrylic acid (L2A1) dyes as well as the preparation procedure of the TiO₂ colloidal solution are described elsewhere.^{4,27,28} The nanostructured dye-sensitized electrodes were prepared as follows: The colloidal TiO₂ solution was first diluted with ethanol (1:1) in order to produce a thin nanostructured TiO₂ film. The TiO₂ solution was thereafter spread out onto conducting SnO₂:F glass pieces, and subsequently heated to 450 °C for 30 min. This produced a 1–2 μm thick nanoporous TiO₂ film. The electrodes were then allowed to cool and thereafter immersed into the dye solutions, 1 mM D9L2A1, 1 mM D5L2A1, 1 mM D5A1, 1 mM L2A1 all dissolved in acetonitrile, for 12 h. The samples were finally rinsed in acetonitrile before dried in air and put in the PES analyzing chamber within ten minutes. For this sample preparation procedure a recent core level PES study showed monolayer formation of D5L2A1 and D9L2A1 on the TiO₂ surface.²⁰ Moreover the molecules had a molecular surface orientation with the cyanoacrylic acid anchor moiety close to the TiO₂ substrate and the triphenylamine moiety pointing out from the surface.²⁰

The D9L2A1, D5L2A1, and D5A1 multilayer samples were prepared by smearing out the respective dye powder onto a F:SnO₂ substrate. The formation of a complete coverage is confirmed from the substantial decrease in the PES Sn signals.

2.2 Measurements

The PES, RPES and XAS measurements were performed using synchrotron radiation at beam line I411 at the Swedish national laboratory MAX-lab in Lund. The electron take-off angle was 70° and the electron take-off direction collinear with the e-vector of the incident photon beam. The kinetic energy of the photoelectrons were measured using a Scienta R4000 WAL analyzer. N 1s XAS spectra were recorded by detection

of secondary electrons in partial yield mode and intensity-normalized *versus* the number of incident photons. The PES spectra were energy-calibrated by setting the Ti2p substrate signal to 458.56 eV and the N 1s XAS spectra energy-calibrated through measurement of the Ti3p peak using first and second order light. The powder samples were energy-calibrated by putting the peak with lowest binding energy at the same position as in the dye-sensitized TiO₂ sample. The PES and N 1s XAS spectra has an overall resolution better than 0.2 eV.

The XES measurements were performed at the undulator beamline I511-3 at MAX II (MAX-lab National Laboratory, Lund University, Sweden), comprising a 49-pole undulator and a modified SX-700 plane grating monochromator. The XES spectra were measured with a high-resolution Rowland-mount grazing-incidence grating spectrometer with a two-dimensional multichannel detector. The XES spectra were measured at 20° incidence angle to avoid self-absorption effects.²⁹ The XES spectra are intensity normalized *versus* total intensity. The XES spectra has an overall resolution of 0.6 eV.

3. Theory

Density functional (DFT) calculations with gradient-corrected exchange and correlation functionals were performed to study the electronic structure of the isolated molecules depicted in Fig. 1 and in addition also on the isolated D5 subunit. Geometry optimization, photoemission and X-ray spectrum calculations were done using the StoBe-deMon code³⁰ with pure density functionals^{31,32} and double-zeta valence basis sets including polarization functions.³³

To ensure a localization of the core-hole in the case of core-excitations, all other atoms of the same element, as the target of the core-excitation, were described by effective core-potentials.^{30,34} The electronic relaxation in the presence of the core-hole was converged using a flexible IGLO basis set³⁵ on the core-excited atom.

For comparison to the experimental photoemission spectra, we derived the density of states (DOS) from electronic ground state calculations. The total DOS was decomposed into different partial DOS (PDOS) for units in the dye molecules by projection onto groups of N,C,O and S atoms in a Mulliken analysis. A constant shift of all calculated DOS curves were added for direct comparison to the experimental spectra.

The XES spectra were derived from the Kohn–Sham orbitals in an electronic ground state calculation; whereas the XAS spectra required calculations with the half core-hole transition potential method^{36,37} in combination with a double-basis set procedure in which, after convergence, the basis set was augmented with a large diffuse basis set for an improved description of the Rydberg and continuum states.^{38,39} For direct comparison to experiment an additional ΔKohn–Sham correction⁴⁰ to the lowest core-excited state was used to shift the entire XAS spectrum.

4. Results and discussion

4.1 Valence electronic structure

4.1.1 Experimental valence spectra. The valence photoelectron spectra for molecular multilayers and surface

adsorbed monolayers can be used to experimentally investigate the density and character of the highest occupied energy states. The experimental valence spectra of both dye-sensitized TiO₂ (molecular monolayer) and multilayer samples of the D9L2A1, D5L2A1, D5A1, and L2A1 dyes are displayed in Fig. 2, together with measurements on the bare TiO₂. The measurements were taken using a photon energy of 100 eV. A first observation from a comparison between the spectra is the absence of the characteristic TiO₂ substrate O2s peak at a binding energy of approximately 23 eV in the spectra of the D9L2A1, D5L2A1, and D5A1-sensitized samples. This shows that the contribution from the substrate to the valence spectra of these samples in Fig. 2 is negligible. In the case of L2A1 sensitized TiO₂ the characteristic O2s peak is observed, and included in Fig. 2 is therefore a L2A1 difference spectrum where the TiO₂ contribution has been subtracted by normalizing to O2s. We also note that the TiO₂ substrate show minor contributions at low binding energies, with a valence band edge located well below 3 eV.

The valence spectra of all the monolayer as well as the multilayer samples for D9L2A1, D5L2A1 and D5A1 show large similarities with each other but are clearly different from L2A1. Specifically, the spectral features at binding energies of 8 eV and higher (E–H) are very similar and this shows that this part of the spectra is largely dominated by the D5/D9 unit. At binding energies lower than 8 eV we observe some spectral changes in the features referred to as A–D. Starting with the two most intense features (C and D) in the region 4–8 eV the spectra for D5L2A1 and D5A1 are similar with one peak observed at about 6.7 eV (D) and one around 3.8 eV (C), although the binding energy position for the latter is slightly higher in D5A1. In comparison, the structure for D9L2A1 is clearly different, with the D structure split into two and the C structure distributed over a larger energy range in the monolayer spectra. This difference for D9L2A1 is thus attributed to the presence of the methoxy groups.

The outermost occupied energy levels are important for electron transfer processes and thus for the function in molecular devices such as solar cells. In Fig. 3 a close-up of the experimentally measured lowest binding energy region is shown. Specifically, this region includes the position of the HOMO (highest occupied molecular orbital) levels for D9L2A1, D5L2A1, D5A1, and L2A1. It is observed that the outermost occupied energy levels differ both in binding energy position and in shape for the different dyes. The molecules possessing the D5/D9 unit all have clearly separated spectral features (A and B) located between 1–2 eV in binding energy whereas no such peak is observed for L2A1. It is therefore concluded that this structure largely originate from the D5/D9 unit and that it can be spectroscopically observed.

The binding energy position of the outermost peak (A) (HOMO), visible in Fig. 3 (and summarized in Table 1), is highest for the D5A1 followed by D5L2A1 and D9L2A1. The difference in binding energy is approximately 0.2 eV between D5A1 and D5L2A1, showing that the insertion of the L2 unit shifts the HOMO level by 0.2 eV towards lower binding energies. The difference between the HOMO of D5L2A1 and D9L2A1 is approximately 0.25 eV, showing that the HOMO

level is further shifted towards lower binding energies by the attachment of methoxy groups on the D5 unit.

The detailed structure of the outermost feature is also different for the three dyes possessing the D5/D9 unit. Starting with the dye sensitized samples (●), the D5A1 molecule has a single peak (A), whereas for the D5L2A1 molecule clearly two peaks (A and B) are visible in the outermost occupied energy level region, see Fig. 3. The experimentally measured binding energy difference between the two peaks of D5L2A1 is 0.5 eV in the TiO₂ sensitized samples. In the case of the D9L2A1 outermost peak structure one main peak is observed. However, in comparison with D5A1, the single peak of D5A1 has a more pronounced dip at the higher binding energy side of the peak compared to that of D9L2A1. This finding clearly indicates the presence of some structure at this binding energy region (B) also in the case of D9L2A1 in similarity with that of D5L2A1.

Interestingly, when comparing the outermost structure of the dye sensitized and multilayer samples of D5L2A1, it is observed that the binding energy difference between structure A and B is different, see Fig. 3. The binding energy difference is approximately 0.2 eV larger in the multilayer sample, clearly showing that the adsorption and organization has a profound effect on the outermost structures.

4.1.2 Theoretical DOS and PDOS. Before comparing experimental and theoretical results, we will briefly describe the electronic structure in D9L2A1, D5L2A1, D5A1 and L2A1 from a series of density functional (DFT) calculations made on single molecules. The emphasis is to dissect the underlying contributing atomic character and distributions of the valence occupied energy levels in a way that can be used for further understanding of the experimental map obtained from the spectroscopic measurements.

The theoretically calculated valence spectra, *i.e.* the total density of states, TDOS, are displayed in Fig. 4. In line with the discussion of the experimental spectra, the labels A'–E' are used to describe the spectra and with A' referring to the HOMO feature. As expected some similarities are observed for D9L2A1, D5L2A1 and D5A1, while L2A1 is clearly different and the discussion below will mainly focus on the three former dyes.

Starting from the D5L2A1 molecule the different features are labeled in Fig. 4a. Specifically we observe two peaks (A' and B') in the binding energy region 1–3 eV and three pronounced structures (C', D' and E') in the binding energy region 3–8 eV. The total density of state are subdivided into partial density of states, PDOS, for the D5 unit, the L2 unit and the A1 unit in order to further resolve the different contributions. The PDOS for the D5 unit in D5L2A1 largely follows the A'–E' TDOS structure, while that of A2 and L1 mainly shows similarities with respect to C' and B' and minor PDOS in A'. Specifically this shows that states B' and C' are distributed over all three units while structure A' is mainly centered on the D5 unit. The effect from the methoxy groups can be followed by a comparison between the TDOS for D9L2A1 and D5L2A1. At lower energy, a shift in states A' and B' towards higher energies is observed. For state C' the effects are smaller while clear differences are observed in the

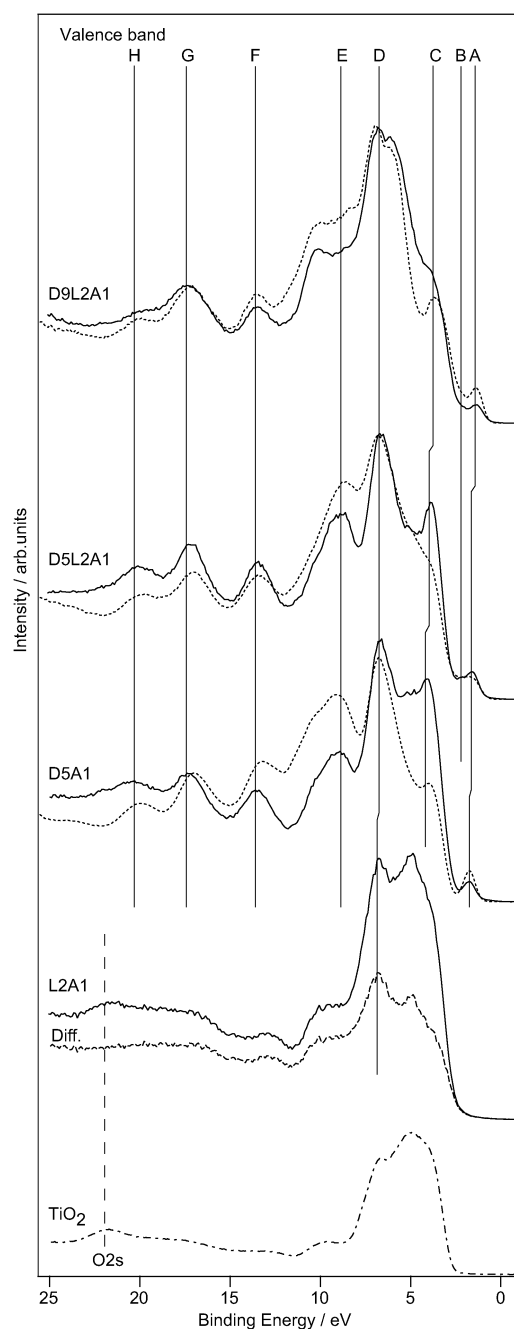


Fig. 2 Valence spectra of both dye-sensitized TiO₂ samples (solid line) and multilayer samples (dotted line) of D9L2A1, D5L2A1, and D5A1. Included is also the valence spectra of dye-sensitized sample of L2A1, bare TiO₂, and the difference spectrum (- -) between the L2A1 sensitized TiO₂ and the bare TiO₂ spectra. The spectra were measured using photon energy of 100 eV.

region of structure D'. In this region a new structure appear originating from rather local states centered on the methoxy groups, as observed from the methoxy PDOS calculation and is in Fig. 4b referred to as O-PDOS in D9.

Comparing TDOS for D5L2A1 and that obtained for the L2A1, larger differences are observed and we specifically point out the absence of state A' in L2A1. The position of HOMO for L2A1 is instead located at an energy close to the C'.

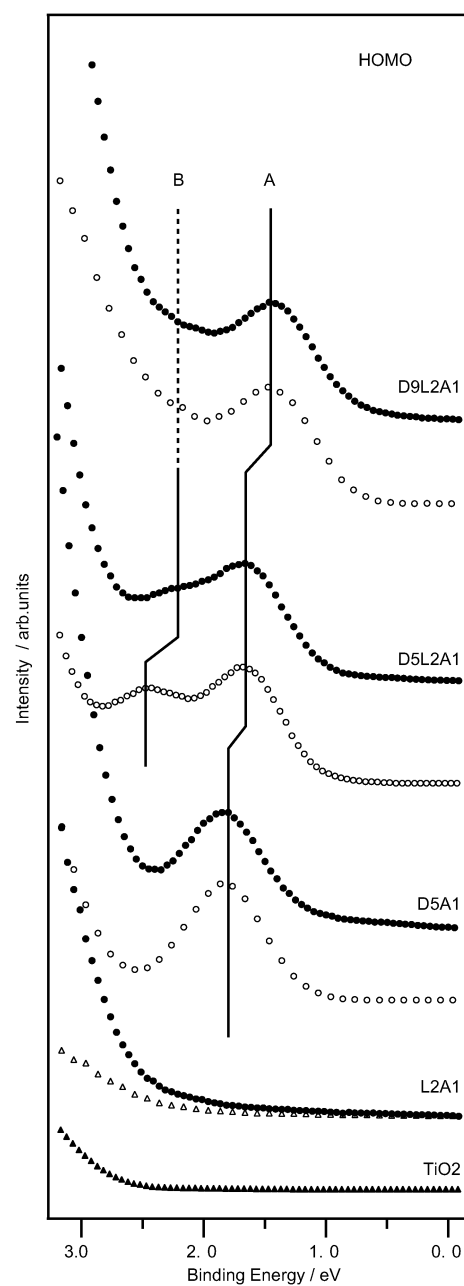


Fig. 3 Spectra of the outermost valence region, showing the HOMO energy levels of the D9L2A1, D5L2A1, D5A1, and L2A1 dye-sensitized TiO₂ surface (●) and multilayer samples (○), measured using photon energy of 100 eV. TiO₂ spectrum (▲) measured using photon energy of 100 eV and the difference spectra (Δ) between the valence spectra of L2A1 and TiO₂.

Moreover, from a comparison between TDOS for D5L2A1 and that obtained for D5A1, the effect from L2 at lower binding energies is mainly a shift of state A' and of the appearance of a new state (B') at a binding energy of about 2.3 eV.

Looking at the N and O PDOS Fig. 4b we note the following: with respect to nitrogen the HOMO level have a clear D5/D9 nitrogen character in the HOMO level, while the N PDOS in the cyanoacrylic is rather localized to a position between C' and D'. With respect to the oxygen in the A1 unit

Table 1 The experimental binding energies of the N 1s core levels, the photon energies for the experimentally measured XAS resonances, the binding energy position of the unoccupied energy levels calculated from experimentally obtained data, the binding energy position of the HOMO level (A), and the binding energy difference between A and Y_A for the dye-sensitized TiO₂ samples

Feature	D9L2A1/eV	D5L2A1/eV	D5A1/eV	L2A1/eV
N 1s _{D5}	399.60	399.75	399.89	—
N 1s _{A1}	398.51	398.51	398.82	399.10
X _A	398.4	398.4	398.5	398.5
X _B	399.6	399.6	399.6	399.7
X _C	400.5	400.5	400.5	400.5
X _D	402.7	402.5	402.3, 403.1	—
Y _A	0.11	0.11	0.32	0.6
Y _B	-1.1	-1.1	-0.78	-0.6
Y _C	-2.0	-2.0	-1.68	-1.4
Y _D	-3.1	-2.8	-2.5, 3.3	—
HOMO (A)	1.41	1.66	1.85	—
$\Delta E_{B(A - Y_A)}$	1.3	1.55	1.53	—

(i.e. in -COOH), no contributions are observed in state A' and B' nor in the HOMO energy of L2A1.

4.1.3 Comparing experimental valence spectra and theoretical DOS. Generally some insight into the complex experimental valence spectrum can be obtained by comparison with theoretical DFT calculations. Such a comparison is shown in Fig. 5. It is observed that the experimental and theoretical spectra are generally in reasonable agreement for all molecules. Most main peaks in the experimental spectra are reproduced in the theoretical spectra showing that the models used are capturing the essential aspects of the dyes, although we expect a broadening in the experimental spectra due to local variations in geometries and intermolecular interactions. The comparison between theory and experiment would be improved by stretching the theoretical energy scale, and a possible explanation to this is that the electron relaxation energy upon valence ionization increases with binding energy. This is a final state effect, which we neglect in the present initial state approximation. The similarity between theory and experiment motivates the following schematic model of the experimental spectra, see Fig. 6.

As a starting point we take the electronic structure of the triphenylamine moiety alone (a single D5 unit) calculated and shown in Fig. 4 and schematically drawn in Fig. 6. The electronic structure may be divided into three main parts, one single level at lower binding energy largely containing the nitrogen lone pair (A'), one set of levels shifted a couple of eV containing a mix of the three phenyl centered π -orbitals (C') and second set of π -orbitals shifted another few eV (D'). Essentially this structure (A, C, and D) is observed in the experimental spectrum of D5A1, although some contributions from the A1 unit (specifically the cyano group, see below) is expected between C and D. As observed in both the theoretical and experimental results discussed above, the incorporation of the thiophene unit L2 in the D5L2A1 molecule gives rise to a new feature (B' and B respectively) at low binding energy. According to the calculations this arises from a mixing of π energy levels in D5 with the HOMO π levels of the thiophene which splits off part of the π manifold structure C to a well-defined level B. At higher binding energies only small

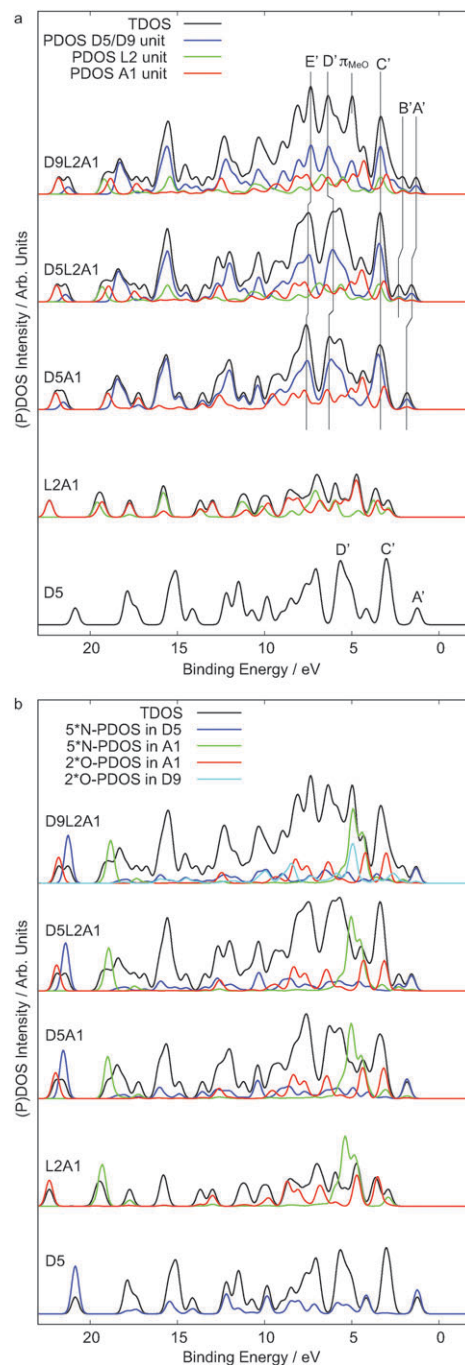


Fig. 4 Calculated density of states of D9L2A1, D5L2A1, D5A1 and L2A1. (a) The total DOS decomposed into partial DOS of the molecular subunits to resolve the electronic structure. (b) The density of states projected onto specific atoms.

differences are observed in the experimental valence spectra as well as the theoretical DOS when comparing D5L2A1 and D5A1. Finally, we note that the experimentally observed effect from the methoxy groups was followed in the theoretical calculations. The direct effect from the presence of the methoxy group is observed in the broadening of state D while the shift of HOMO and HOMO-1 is mainly an inductive effect, since the direct contribution from the methoxy group in these states is very limited (see Fig. 4 and 6).

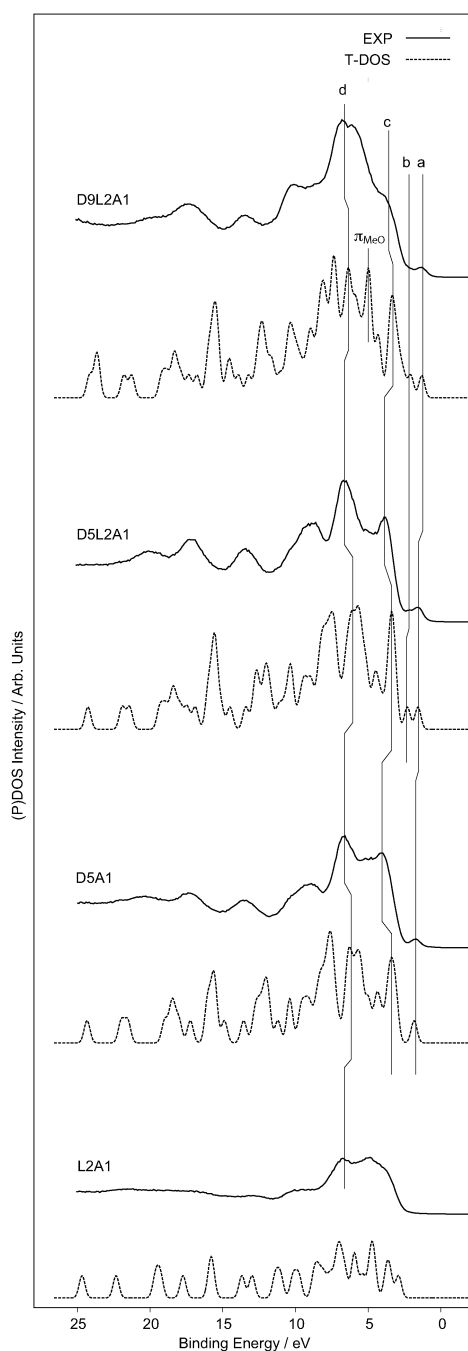


Fig. 5 Experimental monolayer valence spectra (solid lines) and calculated density of states (dashed lines) of D9L2A1, D5L2A1, D5A1, and L2A1. The intensity in the experimental spectra is scaled to fit theory, and the theoretical spectra are shifted by 3.4 eV to align to experiment. Line a refers to the experimental position A and the theoretical position A' in respective spectra.

4.2 The unoccupied states followed by N 1s XAS spectroscopy

The PES data on the occupied energy levels is combined with X-ray absorption spectroscopy (XAS) to probe the unoccupied space and a complete picture of the electronic structure is thus obtained. The nitrogen K-edge (N 1s XAS) allows us to resolve local projections of the unoccupied states onto the nitrogen containing D5/D9 and A1 units. D5/D9 and

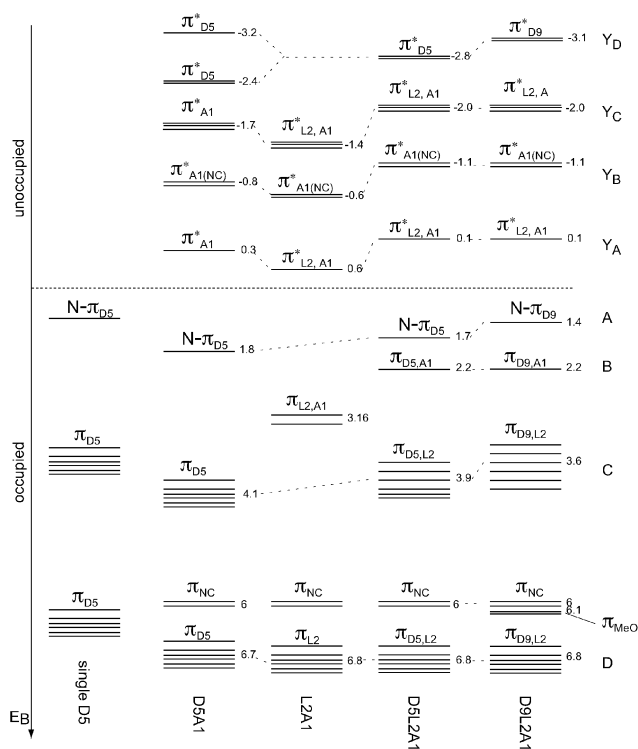


Fig. 6 Schematic picture of the frontier electronic structure of the D9L2A1, D5L2A1, D5A1, and L2A1 sensitized TiO₂ samples. The experimental binding energies are indicated to the right of the different states. The binding energy in the occupied electronic structure are obtained from PES spectra. The unoccupied electronic structure are based on the XAS spectra and their binding energies are determined by combining N 1s-XAS and PES N 1s core level spectra (see text). Comparison between spectra of the different moieties determined the character of the features. The character of the different features in the electronic structure was further determined by RPES and XES in combination with calculations. Included in the picture (left) is also a schematic picture of the calculated occupied energy levels of the D5 unit. The number of levels in each state (A – D, Y_A–Y_D) are also shown schematically.

A1 are natural targets being the functional groups involved in the charge transfer excitation for visible light absorption (see below).⁵

The experimental N 1s XAS spectra of the D9L2A1, D5L2A1, D5A1, and L2A1 sensitized TiO₂ samples together with that of the dye multilayer samples are shown in Fig. 7a, where the absorption intensity is plotted *versus* photon energy. The peaks in the feature below 401 eV in Fig. 7 are denoted X_A, X_B and X_C. It is observed that all monolayer samples (solid line) and multilayer samples (dashed) have two sharp resonance features at approximately the photon energies 398.4 eV and 399.6 eV. The third peak around 400.5 eV varies with the coverage and is least pronounced for L2A1. Since the L2A1 molecule possesses these resonances it is concluded that this feature originates from a resonance centered at the nitrogen atom in the A1 unit.

Furthermore, all N 1s XAS spectra of the dye sensitized samples, except for L1A1, contain a broad resonance, denoted X_E, at higher photon energies, 405–415 eV, and thus, it is concluded that this resonance structure is mainly generated in

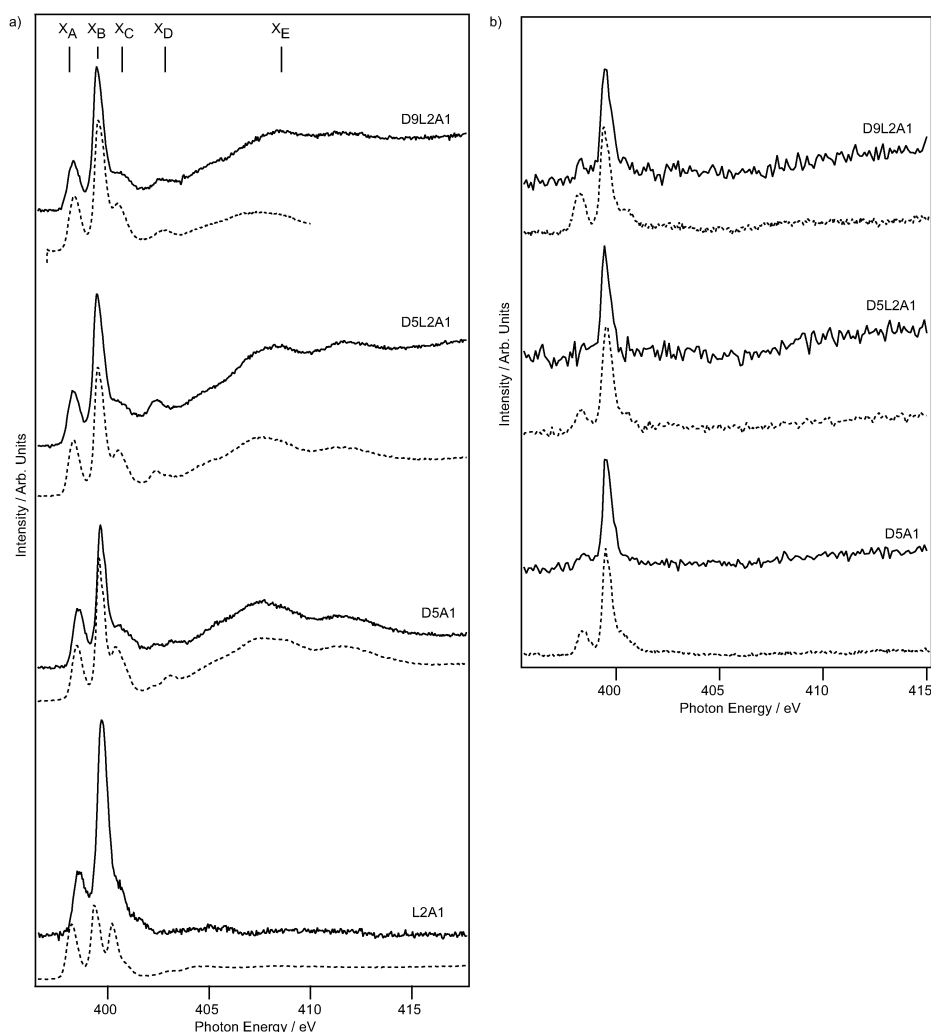


Fig. 7 XAS spectra (left) and integrated (between 5.5–6.5 eV in binding energy) RPES spectra (right) of the D9L2A1, D5L2A1, D5A1, and L2A1 dye-sensitized TiO₂ (solid line) and multilayer samples (dotted line), measured over the nitrogen K-edge.

the D5/D9 units of all molecules, which has previously been shown for D5L2A1.⁵

At intermediate excitation energies around 402–403 eV, there is a feature, X_D, which varies between mono and multilayer coverage and possibly splits for the D5A1 dye. Previous measurements on triphenylamine based molecules has shown resonances at this position,⁵ and since this structure is rather weak in L1A1 the result indicate that also X_D for D9L2A1, D5L2A1, and D5A1 corresponds to states in the triphenylamine N 1s XAS.

The assignments of the experimental N 1s XAS spectra in Fig. 7 are also confirmed by theoretical calculations presented in Fig. 8. The strongest peak, X_B, is in the calculations assigned to the in-plane anti-bonding C=N orbital. It gives a strong signal, since it is a localized state and is not interacting with the conjugated π system. In contrast, the X_A and X_C peaks arise from the out-of-plane anti-bonding C=N orbital which overlaps and contribute to the conjugated π system. In particular the X_A level arise from an orbital that mixes strongly all the way to the triphenylamine moiety. In the theoretical calculations of the N 1s_{A1} contribution to the

XAS spectra the third peak, X_C, is clearly visible and located at approximately 400.5 eV. Interestingly, this resonance peak is clearly visible also in the spectra measured on the multilayered samples whereas it can only be seen as a shoulder in the spectra measured on the dye-sensitized sample, see Fig. 7.

When comparing the dye-sensitized and multilayered N 1s XAS spectra in Fig. 7, the most striking difference is the measurement for the L2A1 molecule. Instead of a dominant resonance at 399.6 eV, the N 1s XAS spectrum for the multilayer contains three peaks with equal intensity. This is a clear indication of a substantial electronic change in the molecule, which we attribute to intermolecular interactions. A possibility could be molecule–molecule interactions for the anchor moieties involving hydrogen bonding with the NC nitrogen atom as previously discussed by Kitamura *et al.*⁶ Unfortunately, the photoelectron spectrum is not available for multilayer L2A1, which would enable us to explore this hypothesis. Ideally we would have preferred to also address the changes observed in the X_C feature in the dye-sensitized and multilayered samples of D9L2A1, D5L2A1, and D5A1

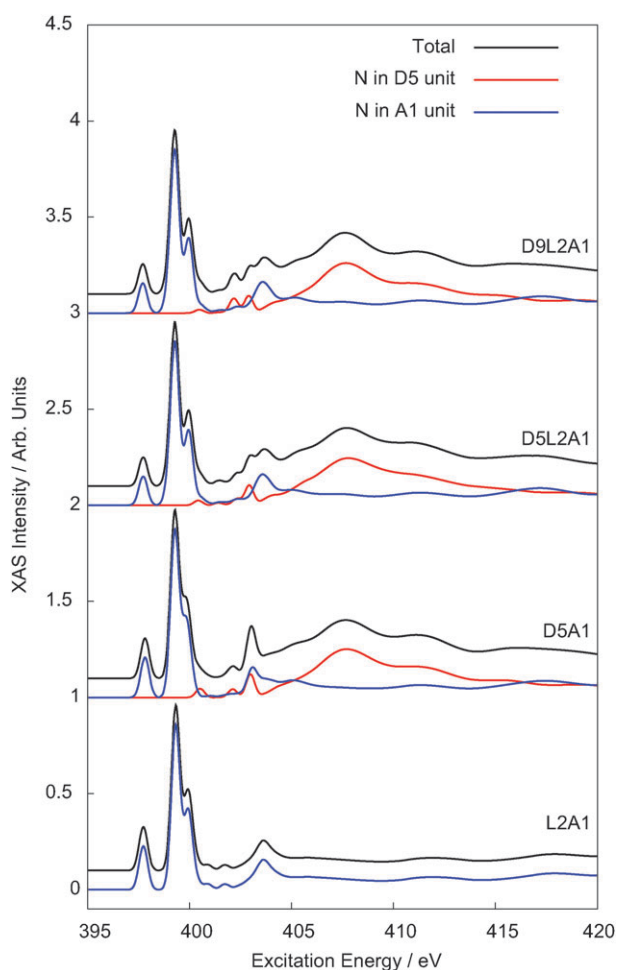


Fig. 8 Theoretically calculated N 1s XAS spectra for the dyes in Fig. 1. The contribution to the N 1s XAS spectra from the nitrogen in the D5/D9 unit and in the A1 unit are also included.

with modeling. At the present stage, however, we have too little structural information about these phases to create constraints when building the models to reach a conclusive statement.

The XAS process involves an electronic excitation from the N 1s core level to an unoccupied energy level, and in a procedure of positioning the unoccupied energy levels on the binding energy scale information about the respective core level is necessary. The binding energy positions of the N 1s core levels related to the D5 and A1 units in the D9L2A1, D5L2A1, and D5A1 are summarized in Table 1. By subtracting the XAS resonance energy from the corresponding core-level binding energy, the position of the unoccupied energy level of the molecules in the presence of a N 1s core hole is obtained. Using this procedure the energy level positions Y_A – Y_D corresponding to the X_A – X_D resonances are calculated and displayed in Table 1. These positions are also schematically drawn in Fig. 6.

Starting with the L2A1 in Fig. 6, three unoccupied energy level positions, Y_A – Y_C , with excited electrons localized at the A1 unit, are experimentally observed. In comparison to L2A1, Y_A – Y_C in D5L2A1 are shifted towards lower binding energies. Moreover, an additional energy level position Y_D connected

with the D5 unit is observed at a binding energy approximately 4.5 eV lower than the HOMO. In the D5L2A1 molecule, Y_A – Y_C are located at lower binding energies compared to D5A1, showing the effect of introducing the L2 unit. Moreover, for D5A1 Y_D is experimentally observed to be split into two, one located higher and one lower compared to Y_D in D5L2A1. Continuing by comparing the D5L2A1 to D9L2A1 in Fig. 6, it is observed that Y_A – Y_C are located at the same energies in both molecules, whereas Y_D is shifted by approximately 0.3 eV towards lower binding energy in D9L2A1 compared to in D5L2A1. Interestingly, the binding energy difference between Y_D and the HOMO is the same in both D9L2A1 and D5L2A1. Together these results show that the methoxy units affect the outermost energy levels corresponding to the D5/D9 unit, while leaving the energy levels corresponding to the A1 rather unchanged.

The binding energy difference between the highest occupied and lowest unoccupied energy levels, *i.e.* between A and Y_A in Fig. 6, in the D9L2A1, D5L2A1, and D5A1, is expected to be involved in the optical transitions observed in the visible region and are, thus, important for the functional properties of these molecules. This binding energy difference, ΔE_B (A – Y_A), is calculated and displayed in Table 1. It is observed that ΔE_B (A – Y_A) is approximately 0.2 eV smaller for D9L2A1 compared to both D5L2A1 and D5A1, implying a redshift of a corresponding UV-vis absorption spectrum peak in the D9L2A1 sample, which also is experimentally observed. Generally when comparing measurements of ΔE_B (A – Y_A) to the UV-vis spectra it should be noted that these may differ firstly due to relaxation in the presence of the core hole in the XAS measurements, resulting in a lower position of the LUMO level in the latter case, and secondly the mixing of other transitions and/or vibrational overtones in the UV-vis spectra. Absolute comparisons of the ΔE_B (A – Y_A) measured with the different procedures should therefore be avoided and instead relative differences are compared. The observed ΔE_B (A – Y_A) between D9L2A1 and D5L2A1 is in line with previously observed UV-vis results showing a redshift of approximately 0.15 eV for the absorption maximum of D9L2A1 compared to D5L2A1 (in acetonitrile).²⁷ However, UV-vis measurements have shown a 0.17 eV blue shifted absorption maximum in the case of D5A1 compared to D5L2A1, which was different from the ΔE_B (A – Y_A) values observed here.⁴¹

4.3 Experimental map of molecular orbital composition

4.3.1 Resonant and non-resonant XES at the nitrogen K-edge. The decay processes from states formed from single photon X-ray excitation or X-ray ionization can be used to experimentally map the PDOS for a molecule with elemental and site specificity.^{42,43} In non-resonant X-ray emission (XES) obtained from a core ionized state (*i.e.* N 1s, in the measurements presented here), the spectrum is described as an emission in a dipole transition between the core ionized and the valence ionized state. The local nature of the core hole makes the technique element specific, largely probing the PDOS for a specific element (*i.e.* N 2p). In resonant XES (or resonant inelastic X-ray scattering, RIXS), the incoming

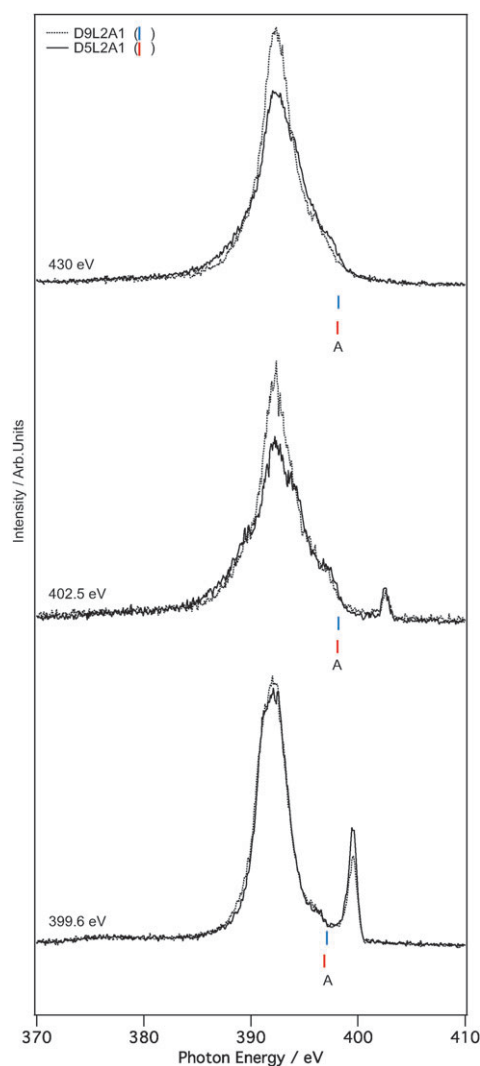


Fig. 9 Experimental XES spectra of D9L2A1 and D5L2A1 sensitized TiO₂ samples, and RXES spectra where the excitation energies were tuned to the XAS resonances X_B (399.6 eV) and X_D (402.5 eV). The position of feature A (HOMO) is shown for D9L2A1 (blue) and D5L2A1 (red).

photon energy can be selected to match a particular site sensitive absorption energy (*e.g.* N 2p in the NC group). In this case the emission is not just element specific but will reflect the PDOS projected onto a specific atomic site.

The N 1s XES spectra for D5L2A1 and D9L2A1 sensitized TiO₂ samples are displayed in Fig. 9. Starting with the non-resonant XES spectra, we observe a main structure with emission energy of about 392 eV for both D5L2A1 and D9L2A1. At energies up to the high-energy cut-off 399 eV some structure in the emission intensity is visible, while at higher energies no emission is observed. The binding energy difference between the HOMO level and the N 1s core level with highest binding energy (*i.e.* N 1s originating from the triphenylamine moiety) is 398.2 and 398.1 for D9A2L1 and D5A2L1 eV, respectively. Thus these measurements indicate the presence of N 2p all the way to the HOMO level, but that most of the N 2p PDOS is positioned about 6 eV below the HOMO energy.

Resonant XES spectra measured at 399.6 and 402.5 eV, *i.e.* the photon energies in the XAS spectra selected to coincide with X_B and X_D respectively, are also shown in Fig. 9. In the figure also the experimental position of the HOMO level are indicated, and these are positioned at an energy obtained from the difference in binding energy between the respective peak and the probed N 1s core level. At the bottom of Fig. 9, the spectra are shown where the excitation energy was tuned to the main XAS peak at X_B (399.6 eV). For both D5L2A1 and D9L2A1 molecules this energy corresponds to the XAS resonance X_B with mainly NC character. Both resonant XES spectra are very similar and have a main peak at 392 eV, indicating that the N 2p DOS from the NC group largely appear about 5.8 eV above the HOMO binding energy. Interestingly both spectra also show a small but clear structure at 396 eV, while no clear structures are observed at higher energies. Referencing this to the HOMO energy, the results indicate that the HOMO (feature A) has a character not distributed over the NC group but that some contribution may be present in states at higher energies. This is in line with the theoretical PDOS results and thus support the position of π_{NC} displayed in Fig. 6.

In the middle of Fig. 9, the resonant XES spectra are also shown where the excitation energy was tuned to XAS feature X_D (402.5 eV). For both D5L2A1 and D9L2A1 molecules, this energy largely matches the energies of the XAS resonances having mainly D5/D9 character. Generally both spectra are rather similar although the shoulder at higher energies is slightly more pronounced in D5L2A1 compared to D9L2A1. Comparing these spectra to those measured at 399.6 eV, an interesting difference is the slight increase in intensity at higher energies. Since this increase in emission coincides with the position of HOMO energy, this indicates the contribution from D5/D9 nitrogen in HOMO (A). Specifically this may be attributed to the mixing of the triphenylamine nitrogen lone pair to the HOMO level and again the result supports the labeling in Fig. 6.

The calculated N 1s XES spectra for the nitrogen atoms in the cyano and phenylaniline group in D5L2A1 and D9L2A1 support this conclusion as is displayed in Fig. 10. The cyano group gives rise to the distinct XES feature seen experimentally measured at 399.6 eV, and a small shoulder at higher emission energies. This shoulder is present also in the measured resonant XES.

The theoretical XES spectra based on the N in the D5/D9 unit show a broad distribution with N 2p character due to conjugation. There is a small effect from the methoxy group, but it is not sufficient to explain the experimental difference in the non-resonant XES of the D5L2A1 and D9L2A1 molecules. Notice that the HOMO orbitals in the XES spectra for the nitrogen atoms in A1 and D5 units occur at different emission energies, because of the difference in N 1s core-level binding energies. The HOMO in the N 1s XES for D5/D9 unit is however clearly observed in the total non-resonant XES spectrum, which qualitatively reproduces the experimental spectrum. Thus, the theoretical results support the conclusion that the emissions found at the highest energies in the non-resonant spectra originate from the D5/D9 unit and that HOMO level contains some D5/D9 lone pair nitrogen

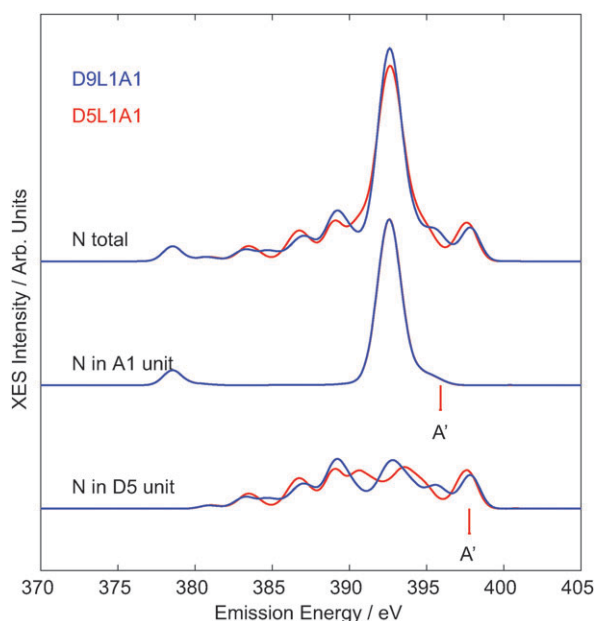


Fig. 10 Calculated XES spectra (N 1s) of the isolated D5L2A1 and D9L2A1 dyes. Spectra is calculated for the non-resonant N 1s XES (top), and also for the resonant N 1s XAS from the A1 unit (middle) and from the D5/D9 unit (bottom).

character. Based on the theoretical calculations we cannot explain the experimental difference between D5L2A1 and D9L2A1 in terms of differences in the electronic structure. This could be due to limitations in the model, the experimental resolution, or related to polarization dependence in the experiment. Further experiments are required to resolve this issue.

4.3.2 Resonant PES at the nitrogen K-edge. Resonant photoemission spectroscopy (RPES) implies photoemission spectroscopy using a photon energy that coincides (resonance) with the excitation energy of a core orbital to an unoccupied orbital in the system (*e.g.* energies in the N 1s XAS spectrum), see Fig. 6. The excited states formed from the X-ray absorption process primarily decay in an Auger type process leading to electron emission. In analyzing the various features it is useful to classify the RPES transitions into spectator and participator processes. The former imply that the decay occurs without direct involvement of the resonantly excited electron, leading to final states having two holes among the valence orbitals in addition to the excited electron and a signal that is constant in kinetic energy. The participator decay, on the other hand, implies that the resonantly excited electron participates in the decay of the core hole to the final state with an electron in the continuum and one valence hole. Since the final state in the resonant participator decay is the same as in non-resonant photoemission, the participator decay signal is constant in binding energy. Moreover, when scanning the photon energies over the N 1s XAS resonance energies, if neglecting coupling to states on other molecules or to the substrate, the mechanism for RPES predicts that participator decay will enhance only those valence band states which has similar character as the XAS resonance.^{44,45}

Image plots of the experimental valence spectra for D9L2A1, D5L2A1, and D5A1 adsorbed at TiO₂ and taken at the photon energies of the N 1s XAS resonances are shown in Fig. 11. Following the photon energy of the strongest XAS structures, X_B, originating from the NC group (at 399.6 eV for D9L2A1, D5L2A1 and D5A1) we observe a large increase in cross section also in the RPES spectra, in all cases located at a binding energy close to 6 eV, which thus indicate participator contributions. Therefore, the increase in intensity indicates

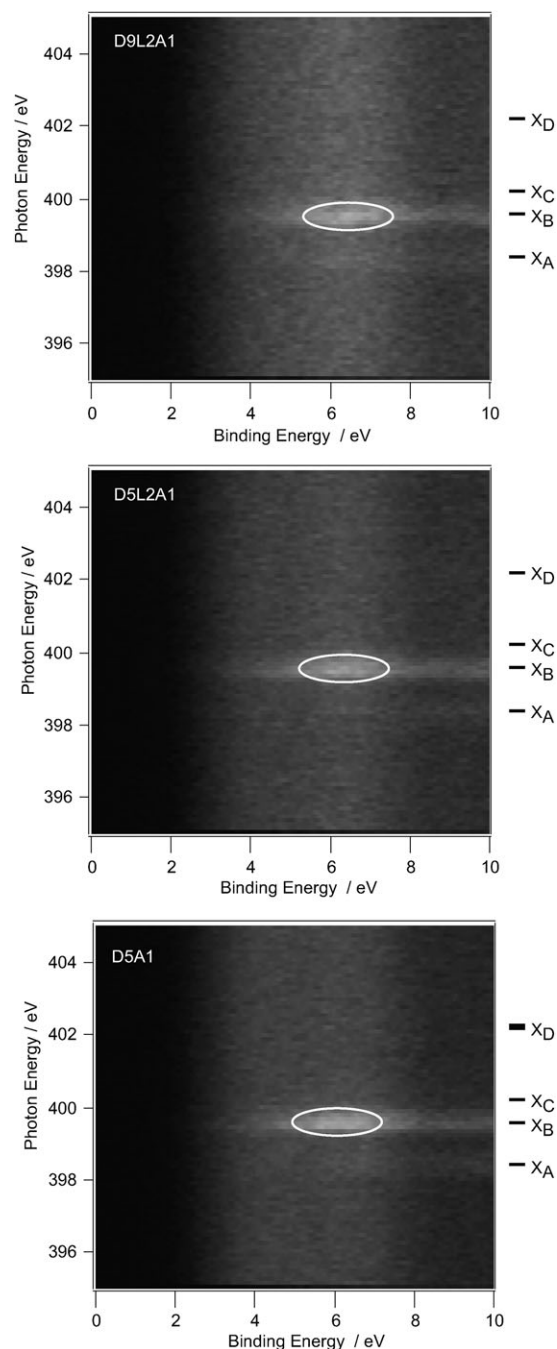


Fig. 11 RPES image plots over the N1s XAS resonance of D9L2A1 (top), D5L2A1 (middle), and D5A1 (bottom) sensitized TiO₂ surfaces. The ring indicates the main participator enhanced valence structures over the NC XAS resonance.

that the π_{NC} contribution to the valence structure is rather localized to a binding energy shifted about 4.5 eV from the outermost valence level. For D9L2A1 and D5L2A1 these experimental results support the findings obtained from XES and thus the experimental position of the NC groups in Fig. 6.

4.4 Femtosecond time development of the excited state

It is also of interest to follow in detail the intensity of a particular valence orbital hole state as a function of photon energy over the energy interval of the XAS spectrum. Preferable the XAS spectrum is measured by recording electrons emitted at the binding energy interval of the valence orbital with dominating participator character. This procedure may allow conclusions to be drawn as to the time development of the electron in the excited state orbital on a few femto-second time-scale. The argument for this is based on the short lifetime of the core hole (6 fs for N 1s).^{45–48} If the electron in the excited state orbital undergoes transfer to a neighbouring unit, molecule or substrate in a time interval short compared to the core hole lifetime, participator transitions will not occur and the corresponding feature in the integrated RPES spectrum will be missing. Hence, in order to study such fs transfer processes an outer valence region (5.5–6.5 eV in binding energy) that is largely dominated by participator decay from the N 2p at the NC group (see above) was chosen. The intensity of this valence orbital will then act as a probe to detect transfer processes from the NC group of the different resonance states in the XAS spectrum.

Fig. 7 shows a comparison between the integrated RPES and XAS spectra for multilayer and monolayer of D9L2A1, D5L2A1, and D5A1. Based on the local character (see discussion on XAS) of the most intense peak at about 400 eV, this peak was used for normalization. In the calculations, we showed support for this conclusion since it is a localized in-plane π_{NC}^* state not mixed with the conjugated π system. As discussed above, the multilayer and monolayer XAS spectra are very similar for D9L2A1 with the three features at lower energies arising from absorption at the NC group. With respect to the most intense peak, we observe some minor decrease (less than 13%) in relative intensity for the first resonance together with some broadening for the third resonances. These small changes probably reflect some small differences in geometries. Next the multilayer integrated RPES spectrum for D9L2A1 is compared with its XAS multilayer spectrum. The three first resonances are rather similar although the intensity from the first and third has decreased slightly (less than 12%). However at energies above 401 eV large differences are observed. This is to be expected since these resonances have very little π_{NC}^* character, but is instead more localized on the D9 unit.

The next comparison is between the integrated RPES spectrum obtained for a monolayer of D9L2A1 with that of a multilayer. Interestingly, we see clear differences in this case. The spectrum of the monolayer shows one clear resonance structure at 400 eV, and at lower energy (399 eV) a smaller peak is observed in the integrated RPES spectrum for the

monolayer. With respect to the most intense peak we observe a clear decrease of approximately 60% in intensity for the first resonance. Based on the reasoning above our conclusion is, thus, that participator decay is suppressed in the case for the lower-lying resonances compared to the case of the more localized resonance at 400 eV due to more pronounced charge redistribution. Moreover this charge distribution should occur in a timescale of 6 fs. Based on the valence band observed for TiO₂ (Fig. 2 and 3) and the binding energy position determined for Y_A (LUMO), this result is rather surprising with the position of the first resonance within the bandgap of the TiO₂ substrate. In the present case, the presence of the core hole requires special considerations, which make extrapolations of conclusions drawn for the optical regime nontrivial (see discussion above). Still, however, one interpretation is fs transfer to a new state formed from the surface binding and organization, with an energy in the bandgap.

The trends discussed above for D9L2A1 are also observed for D5L2A1 and D5A1. Thus also for these molecules dynamics in the femtosecond time regime are observed. For L2A1 the large difference between the monolayer spectrum and the multilayer spectrum prevent a similar discussion.

5. Conclusions

In this paper we have shown how the element specificity of photoelectron spectroscopy (PES), X-ray absorption spectroscopy (XAS), X-ray emission spectroscopy (XES) and resonant photoelectron spectroscopy (RPES) can be used to map the frontier electronic levels and to delineate the character of the frontier electronic levels for dye molecules (D5A1, D5L2A1, and D9L2A1) containing the triphenylamine moiety (D9/D5), the thiophene moiety (L2) and the cyanoacrylic acid moiety (A1). The molecules were investigated both as molecular monolayers adsorbed on TiO₂ substrate and as multilayers, and the experiments were supported by theoretical DFT calculations. Although the general results from experimental and theoretical determinations of the energy level positions were similar, clear quantitative differences were observed for the dye molecules. Furthermore, some of the results were sensitive to differences in intermolecular interactions as observed when comparing values obtained for multilayer and monolayers.

From the experiments we have obtained a quantitative energy level scheme following the effects from changes in the molecular design. Specifically, the positions of the outermost occupied energy levels were experimentally determined for D5A1, D5L2A1, and D9L2A1. The shift of the HOMO (referred to as A in the paper) when introducing the L2 unit was determined to 0.2 eV, and at the same time a second peak, HOMO – 1 (referred to as B in the paper) appeared. The shift of HOMO due to the methoxy groups in D9L2A1 was determined to be 0.25 eV. The HOMO level showed large triphenylamine character while HOMO – 1 show mixing of the A1 moiety for both D5L2A1 and D9L2A1 molecules. The origin of the low binding energy HOMO – 1 levels in D9L2A1 and D5L2A1 (not observed in D5A1) is the mixing between the D9/D5 π states and the L2 centered π states. For D9L2A1

and D5L2A1 only minor differences were observed in the unoccupied states as measured by N 1s XAS. Based on the local character of the Al centered NC states, a binding energy position shifted about 4.5 eV *versus* the HOMO-level. Interesting effects explained by electron dynamics in the femtosecond time regime were also observed from experimental integrated RPES spectra.

Acknowledgements

The experimental work was supported by the Swedish Research Council (VR), the Göran Gustafsson Foundation, the Carl Trygger Foundation, the Magnus Bergvall foundation, the Knut and Alice Wallenberg foundation, and the Swedish Energy Agency. We thank the staff at MAX-lab for competent and friendly assistance. The theoretical modeling was made possible through generous allocations of computer time through SNIC at the Swedish National Supercomputer Center (NSC) and Center for Parallel Computing (PDC), Sweden.

References

- M. K. Nazeeruddin, A. Kay, I. Rodicio, R. Humphry-Baker, E. Muller, P. Liska, N. Vlachopoulos and M. Gratzel, *J. Am. Chem. Soc.*, 1993, **115**, 6382–6390.
- M. K. Nazeeruddin, P. Pechy, T. Renouard, S. M. Zakeeruddin, R. Humphry-Baker, P. Comte, P. Liska, L. Cevey, E. Costa, V. Shklover, L. Spiccia, G. B. Deacon, C. A. Bignozzi and M. Gratzel, *J. Am. Chem. Soc.*, 2001, **123**, 1613–1624.
- M. K. Nazeeruddin, F. De Angelis, S. Fantacci, A. Selloni, G. Viscardi, P. Liska, S. Ito, T. Bessho and M. Gratzel, *J. Am. Chem. Soc.*, 2005, **127**, 16835–16847.
- D. P. Hagberg, T. Edvinsson, T. Marinado, G. Boschloo, A. Hagfeldt and L. C. Sun, *Chem. Commun.*, 2006, 2245–2247.
- E. M. J. Johansson, T. Edvinsson, M. Odelius, D. P. Hagberg, L. Sun, A. Hagfeldt, H. Siegbahn and H. Rensmo, *J. Phys. Chem. C*, 2007, **111**, 8580–8586.
- T. Kitamura, M. Ikeda, K. Shigaki, T. Inoue, N. A. Anderson, X. Ai, T. Q. Lian and S. Yanagida, *Chem. Mater.*, 2004, **16**, 1806–1812.
- K. Hara, M. Kurashige, Y. Dan-oh, C. Kasada, A. Shinpo, S. Suga, K. Sayama and H. Arakawa, *New J. Chem.*, 2003, **27**, 783–785.
- K. R. J. Thomas, J. T. Lin, Y. C. Hsu and K. C. Ho, *Chem. Commun.*, 2005, 4098–4100.
- K. Sayama, S. Tsukagoshi, T. Mori, K. Hara, Y. Ohga, A. Shinpou, Y. Abe, S. Suga and H. Arakawa, *Sol. Energy Mater. Sol. Cells*, 2003, **80**, 47–71.
- M. Velusamy, K. R. J. Thomas, J. T. Lin, Y. C. Hsu and K. C. Ho, *Org. Lett.*, 2005, **7**, 1899–1902.
- I. Jung, J. K. Lee, K. H. Song, K. Song, S. O. Kang and J. Ko, *J. Org. Chem.*, 2007, **72**, 3652–3658.
- D. Shi, Y. M. Cao, N. Pootrakulchote, Z. H. Yi, M. F. Xu, S. M. Zakeeruddin, M. Graetzel and P. Wang, *J. Phys. Chem. C*, 2008, **112**, 17478–17485.
- S. Ito, H. Miura, S. Uchida, M. Takata, K. Sumioka, P. Liska, P. Comte, P. Pechy and M. Graetzel, *Chem. Commun.*, 2008, 5194–5196.
- M. F. Xu, S. Wenger, H. Bala, D. Shi, R. Z. Li, Y. Z. Zhou, S. M. Zakeeruddin, M. Gratzel and P. Wang, *J. Phys. Chem. C*, 2009, **113**, 2966–2973.
- H. Qin, S. Wenger, M. Xu, F. Gao, X. Jing, P. Wang, S. M. Zakeeruddin and M. Graetzel, *J. Am. Chem. Soc.*, 2008, **130**, 9202.
- M. K. Wang, M. F. Xu, D. Shi, R. Z. Li, F. F. Gao, G. L. Zhang, Z. H. Yi, R. Humphry-Baker, P. Wang, S. M. Zakeeruddin and M. Gratzel, *Adv. Mater.*, 2008, **20**, 4460–4463.
- L. Schmidt-Mende, U. Bach, R. Humphry-Baker, T. Horiuchi, H. Miura, S. Ito, S. Uchida and M. Gratzel, *Adv. Mater.*, 2005, **17**, 813.
- K. R. J. Thomas, Y. C. Hsu, J. T. Lin, K. M. Lee, K. C. Ho, C. H. Lai, Y. M. Cheng and P. T. Chou, *Chem. Mater.*, 2008, **20**, 1830–1840.
- M. F. Xu, R. Z. Li, N. Pootrakulchote, D. Shi, J. Guo, Z. H. Yi, S. M. Zakeeruddin, M. Gratzel and P. Wang, *J. Phys. Chem. C*, 2008, **112**, 19770–19776.
- M. Hahlin, E. M. J. Johansson, S. Plogmaker, M. Odelius, D. P. Hagberg, L. C. Sun, H. Siegbahn and H. Rensmo, *Phys. Chem. Chem. Phys.*, 2010, **12**, 1507–1517.
- T. Marinado, D. P. Hagberg, M. Hedlund, T. Edvinsson, E. M. J. Johansson, G. Boschloo, H. Rensmo, T. Brinck, L. C. Sun and A. Hagfeldt, *Phys. Chem. Chem. Phys.*, 2009, **11**, 133–141.
- E. M. J. Johansson, M. Hedlund, H. Siegbahn and H. Rensmo, *J. Phys. Chem. B*, 2005, **109**, 22256–22263.
- K. Westermark, H. Rensmo, H. Siegbahn, K. Keis, A. Hagfeldt, L. Ojamae and P. Persson, *J. Phys. Chem. B*, 2002, **106**, 10102–10107.
- K. Westermark, H. Rensmo, J. Schnadt, P. Persson, S. Sodergren, P. A. Bruhwiler, S. Lunell and H. Siegbahn, *Chem. Phys.*, 2002, **285**, 167–176.
- G. M. Liu, A. Klein, A. Thissen and W. Jaegermann, *Surf. Sci.*, 2003, **539**, 37–48.
- K. Schwanitz, U. Weiler, R. Hunger, T. Mayer and W. Jaegermann, *J. Phys. Chem. C*, 2007, **111**, 849–854.
- D. P. Hagberg, J. H. Yum, H. Lee, F. De Angelis, T. Marinado, K. M. Karlsson, R. Humphry-Baker, L. C. Sun, A. Hagfeldt, M. Gratzel and M. K. Nazeeruddin, *J. Am. Chem. Soc.*, 2008, **130**, 6259–6266.
- P. Wang, S. M. Zakeeruddin, P. Comte, R. Charvet, R. Humphry-Baker and M. Gratzel, *J. Phys. Chem. B*, 2003, **107**, 14336–14341.
- M. Magnuson, N. Wassdahl and J. Nordgren, *Phys. Rev. B: Condens. Matter*, 1997, **56**, 12238–12242.
- K. Hermann, L. Pettersson, M. Casida, C. Daul, A. Goursoot, A. Koester, E. Proynov, A. St-Amant and D. Salahub, Contributing authors: V. Carravetta, H. Duarte, C. Friedrich, N. Godbout, J. Guan, C. Jamorski, M. Leboeuf, M. Leetmaa, M. Nyberg, S. Patchkovskii, L. Pedocchi, F. Sim, L. Triguero and A. Vela, StoBe-deMon version 2.2, 2006.
- A. D. Becke, *Phys. Rev. A: At., Mol., Opt. Phys.*, 1988, **38**, 3098.
- J. P. Perdew, *Phys. Rev. B: Condens. Matter*, 1986, **34**, 7406.
- N. Godbout, D. R. Salahub, J. Andzelm and E. Wimmer, *Can. J. Chem.*, 1992, **70**, 560.
- L. G. M. Pettersson, U. Wahlgren and O. Gropen, *J. Chem. Phys.*, 1987, **86**, 2176.
- W. Kutzelnigg, U. Fleischer and S. M., *NMR-Basic Principles and Progress*, Springer Verlag, Heidelberg, 1990.
- J. C. Slater, *Adv. Quantum Chem.*, 1972, **6**, 1.
- J. C. Slater and K. H. Johnson, *Phys. Rev. B: Solid State*, 1972, **5**, 844.
- H. Agren, V. Carravetta, O. Vahtras and L. G. M. Pettersson, *Theor. Chem. Acc.*, 1997, **97**, 14.
- L. Triguero, L. G. M. Pettersson and H. Agren, *Phys. Rev. B: Condens. Matter Mater. Phys.*, 1998, **58**, 8097.
- C. Kolczewski, R. Puttner, O. Plashkevych, H. Agren, V. Staemmler, M. Martins, G. Snell, A. S. Schlachter, M. Sant'Anna, G. Kaindl and L. G. M. Pettersson, *J. Chem. Phys.*, 2001, **115**, 6426–6437.
- D. P. Hagberg, T. Marinado, K. M. Karlsson, K. Nonomura, P. Qin, G. Boschloo, T. Brinck, A. Hagfeldt and L. Sun, *J. Org. Chem.*, 2007, **72**, 9550–9556.
- M. Magnuson, L. Yang, J. H. Guo, C. Sathe, A. Agui, J. Nordgren, Y. Luo, H. Agren, N. Johansson, W. R. Salaneck, L. E. Horsburgh and A. P. Monkman, *Chem. Phys.*, 1998, **237**, 295–304.
- M. Magnuson, L. Yang, J. H. Guo, C. Sathe, A. Agui, J. Nordgren, Y. Luo, H. Agren, N. Johansson, W. R. Salaneck, L. E. Horsburgh and A. P. Monkman, *J. Electron Spectrosc. Relat. Phenom.*, 1999, **101–103**, 573–578.

-
- 44 E. M. J. Johansson, M. Hedlund, M. Odelius, H. Siegbahn and H. Rensmo, *J. Chem. Phys.*, 2007, **126**, 244303.
- 45 J. Schnadt, P. A. Bruhwiler, L. Patthey, J. N. O'Shea, S. Sodergren, M. Odelius, R. Ahuja, O. Karis, M. Bassler, P. Persson, H. Siegbahn, S. Lunell and N. Martensson, *Nature*, 2002, **418**, 620.
- 46 O. Bjorneholm, A. Nilsson, A. Sandell, B. Hernnas and N. Martensson, *Phys. Rev. Lett.*, 1992, **68**, 1892–1895.
- 47 P. A. Bruhwiler, A. J. Maxwell, P. Rudolf, C. D. Gutleben, B. Wastberg and N. Martensson, *Phys. Rev. Lett.*, 1993, **71**, 3721–3724.
- 48 W. Wurth and D. Menzel, *Chem. Phys.*, 2000, **251**, 141–149.